Hindawi Publishing Corporation
ISRN Biomaterials
Volume 2014, Article ID 897468, 8 pages
http://dx.doi.org/10.1155/2014/897468

Research Article

Effect of Synthesis Temperature on the Crystallization and Growth of In Situ Prepared Nanohydroxyapatite in Chitosan Matrix

Habiba Elhendawi,[1] R. M. Felfel,[1] Bothaina M. Abd El-Hady,[2] and Fikry M. Reicha[1]

[1] *Biological Advanced Materials, Physics Department, Faculty of Science, Mansoura University, Egypt*
[2] *Biomaterials Department, National Research Center, 33 El-Bohooth Street, Dokki, Cairo 12622, Egypt*

Correspondence should be addressed to R. M. Felfel; reda_felfel@yahoo.com

Received 29 December 2013; Accepted 16 January 2014; Published 24 February 2014

Academic Editors: D. Arcos and N. Hanagata

Hydroxyapatite nanoparticles (nHA) have been used in different biomedical applications where certain particle size distribution and morphology are required. Chitosan/hydroxyapatite (CS/HA) nanocomposites were prepared using in situ coprecipitation technique and the effect of the reaction temperature on the crystallization and particle growth of the prepared nanohydroxyapatite particles was investigated. The composites were prepared at different synthesis temperatures (−10, 37, and 60°C). XRD, FTIR, thermal analysis, TEM and SEM techniques were used to characterize the prepared specimens. It was found that the increase in processing temperature had a great affect on particle size and crystal structure of nHA. The low temperature (−10°C) showed inhabitation of the HA growth in c-direction and low crystallinity which was confirmed using XRD and electron diffraction pattern of TEM. Molar ratio of the bone-like apatite layer (Ca/P) for the nanocomposite prepared at 60°C was higher was higher than the composites prepared at lower temperatures (37 and −10°C).

1. Introduction

Natural bone is a complex inorganic-organic nanocomposite, in which hydroxyapatite [HA, $Ca_{10}(PO_4)_6(OH)_2$] nanocrystallites and collagen fibres are well arranged in a hierarchical architecture [1]. High mechanical strength and fracture toughness of the bone were attributed to reinforcement of flexible collagen fibers with HA nanocrystals [2]. Bone is one of the human body tissues that can be replaced or repaired after fracture [3]. Bone can be repaired by autografts, allografts, or use of implant (e.g., scaffold, screws, nail, and plates). Bone fixation devices have been widely used in order to obviate the complications of autografts and allografts procedures such as infection and pain [4, 5]. Metallic implants have been applied for bone fixation since 1895 [6]. However, bioresorbable polymers such as poly lactic acid, poly glycolic acid, and chitosan were introduced as alternative for metals to overcome the complications of metallic devices such as stress shielding, corrosion, and removal surgery [7].

Bioresorbable polymers have been applied for biomedical application due to their various properties (e.g., biocompatibility, biodegradability, porosity, charge, mechanical strength, and hydrophobicity). Furthermore, they could be chemically modified by change of polymerization conditions and ratios of the monomers within the copolymers [1]. Natural polymers such as chitosan (CS) have been replacing synthetic polymers due to their biocompatibility and nontoxic nature of their degradation products [8]. Chitosan as a biofunctional material offers excellent biocompatibility, biodegradability, and osteoconductive properties. Moreover, it can be degraded enzymatically to harmless products in the human body [9]. The potential applications of chitosan and derivatives were attributed to their cationic nature. Chitosan could be considered as a linear polyelectrolyte with a high charge density which could interact with negatively charged surfaces such as proteins. Thus, these superior properties made chitosan and its derivatives ideal materials for biomedical applications [10].

Polymers showed limited bioactivity and mechanical properties. Therefore, addition of bioactive fillers such as HA or bioactive glass became essential to overcome the limitations of pure polymeric implants. HA can promote the formation of bone-like apatite on its surface (i.e., bioactivity) [11]. Polymer/HA composites showed a good capability of promoting osteoblast adhesion, migration, differentiation, and proliferation [12]. Thus, these composites have a potential for bone repair and regeneration applications. The geometrical dimensions of HA play a crucial role in mechanical and biological performance of the composites. It was reported that use of nanosized HA particles (n-HA) caused a significant increase in protein adsorption and cell adhesion to the surfaces of the scaffold and improved the mechanical and biological properties [13, 14]. Misra et al. [15] reported advantages for the use of bioglass nanoparticles in comparison with microsize, related not only to mechanical properties but also to the bioactivity of the composites. The enhancement in mechanical properties was attributed to increase in the interfacial surface area of nanoparticles [16], whilst the improvement in bioactivity was ascribed to the formation of nanotopography on the nanocomposite surfaces.

Mechanical properties of nanocomposites could be controlled by several parameters such as properties of the matrix and fillers, distribution of the fillers, preparation method, and matrix/particles interfacial bonding. Efficiency of load transfer from the polymer matrix to nanoparticles is mainly dependent on strength of matrix/particle interface. Thus, surface modification of nanoparticles is required in order to promote better fillers dispersion and to enhance the interfacial adhesion between the matrix and the nanophases [17–19].

Dispersion of nanoparticles is the main challenge of preparing nanocomposites. Therefore, in situ synthesis procedure of nHA in chitosan matrix was used in the current study. A few attempts were applied to investigate the effect of processing conditions (e.g., polymer type, temperature, pH, and agitation rate) on the particle size and morphology of insitu prepared HA in polymer matrices. The type of polymer exercises a selective influence on the crystallites size and ratios of detected calcium orthophosphates [20]. The crystallinity and crystallite size of the HA nanoparticles increased with increasing synthesis temperature [21–26]. Martínez-Castañón et al. [27] reported that the prepared HA at higher pH values demonstrated high crystallinity which was attributed to the presence of OH^- groups at high concentration. Salimi et al. [28] found that cuboid-like particles were obtained at lower agitation rates, whilst elongated particles were obtained at high shear (i.e., at high agitation rate) created by the homogenizer. The effect of calcination temperature on particle size of HA was also previously demonstrated [29–31].

This study aimed to investigate the effect of reaction temperature on the particle morphology and size of the CS/nHA nanocomposite using in situ coprecipitation method. This method was used in order to overcome the aggregation of HA nanoparticles.

2. Materials and Methods

2.1. Materials. Chitosan powder was purchased from Acros Organics (USA) with a molecular weight of ~300,000 and N-deacetylation degree of 86%. Calcium hydroxide $Ca(OH)_2$, (ANALAR, UK) and orthophosphoric acid (H_3PO_4, purity 99.9%, Sigma-Aldrich) were used as starting precursors for hydroxyapatite.

Sodium chloride (NaCl), sodium hydrogen carbonate ($NaHCO_3$), potassium chloride (KCl), dipotassium hydrogen phosphate (K_2HPO_4), magnesium chloride hexahydrate ($MgCl_2{\cdot}6H_2O$), calcium chloride ($CaCl_2$), sodium sulfate (Na_2SO_4), Tris-hydroxymethyl aminomethane: $(HOCH_2)_3CNH_2$, and 1 M hydrochloric acid (HCl) were obtained from Fisher Scientific and were used as starting precursors for preparation of SBF solution.

2.2. Preparation of CS/HA Nanocomposite. The chitosan/n-HA composites of weight ratio 30/70 were synthesized by the following procedure. Chitosan solution having a concentration of 3 wt% was prepared by dissolving of chitosan in 2 wt% acetic acid with stirring for 8 h to get a perfectly transparent solution and left overnight to get off the air bubbles. Afterwards, a 10 wt% solution of H_3PO_4 was added to the chitosan solution. The chitosan/H_3PO_4 solution was then dropped at the rate of ~3 mL min^{-1} into the 4% ethanol solution of $Ca(OH)_2$ with mechanical stirring. The titration procedure was performed using ultrasonic apparatus (Fisher Scientific, Model FS9H W/T, USA) filled with water and the temperature was adjusted at $-10^{\circ}C \pm 1.0$ by using a mixture of crushed ice/NaCl (with weight ratio of 3/1) and acetone. Warm water was used to obtain the temperature of $37^{\circ}C \pm 1.0$ and $60^{\circ}C \pm 1.0$. Temperature values were measured using mercury thermometer. The pH was also adjusted to be ~10 using NaOH solution. After titration process, the solution was stirred for 24 h, and then the produced slurry was aged for further 24 h. Finally, the precipitates were filtered and washed several times with deionized water, dried in vacuum oven at 50°C, and stored in a desiccator until characterization. The same procedure was performed at 37°C to prepare pure hydroxyapatite (HA).

2.3. Characterization Techniques

2.3.1. X-Ray Diffraction. The X-ray diffraction (XRD) measurements were performed for HA powder, CS alone, and composite samples using a diffractometer (Bruker Axs D8 Advance, Germany). CuKα radiation (λ = 1.54 Å) was used at voltage of 40 kV and current of 25 mA. The samples were scanned using a step-scanning method with scanning speed of $2\theta = 2^{\circ}$/min in the range from 5° to 55° of the diffraction angle (2θ).

2.3.2. Determination of Crystallites Size and Crystallinity. The average crystallite size (L) was determined using Scherrer's equation [32]:

$$L = \frac{K\lambda}{\beta_{002}\cos\theta}, \quad (1)$$

where β_{002} is the full width at half of the maximum (in rad) of (002) peak, λ is the wavelength of X-ray radiation (1.54178 Å), K is a constant that depends on the crystallite shape (approximately equal to unity).

The percentage of crystallinity (X_c%) can also be calculated by using the following equation [32]:

$$X_c\% = \left(\frac{K_A}{\beta_{002}}\right)^3 \times 100, \quad (2)$$

where β_{002} is the full width at half of the maximum in degree and K_A is a constant (0.24).

2.3.3. Fourier Transform Infrared (FTIR) Spectroscopy Analysis. Identification of functional groups of produced HA and composites was confirmed using FTIR (Nicolet Spectrometer model 670 with a FT-Raman accessory, USA). The specimens were scanned in transmittance mode in the region of 4000 and 550 cm^{-1} (wave numbers) using KBr pellet technique with a resolution of 4 cm^{-1}. Approximately 2 mg of the samples powder was carefully mixed with ~198 mg KBr and pressed into a pellet.

2.3.4. Thermogravimetric Analysis (TGA). The TG analysis was conducted for the specimens using a differential thermal analyzer (Setram Labsys TG-DSC16) under inert gas. A sample size of 6–10 mg was placed into a small platinum crucible and heated from room temperature to 1000°C at the rate of 10°C/min. The weight loss (%) against the temperature of the specimens was determined.

2.3.5. Electron Microscopic Analysis. The prepared n-HA and their dispersion, morphology, and particle size in the chitosan matrix were examined using transmission electron microscopy (TEM). This was performed by a JEOL 2010 (Japan), using an accelerating voltage of 200 kV and a copper electron microscopic grid supported by a porous carbon (mesh size 300) film.

The surface topography of the pure n-HA and the composites was characterized using a scanning electron microscopy (JXA840 JEOL, SEM, Japan) at an accelerating voltage of 15 kV and a working distance of 10 mm. Specimens were sputter-coated with carbon for energy dispersive X-ray (EDX) analysis. EDX test was conducted for the composites after soaking in stimulated body fluid (SBF) for 4 weeks. It was used for determining calcium to phosphate ratio (Ca/P) to confirm the formation of apatite layer on the surface of CS/HA composites.

2.3.6. In Vitro Bioactivity Test. Bioactivity of the produced composites was examined via apatite formation by soaking in SBF solution. SBF solution was prepared according to the procedure presented by Li et al. [33, 34]. The samples were immersed in SBF solution for 4 weeks.

3. Results and Discussion

3.1. X-Ray Diffraction Analysis. Figure 1 shows the XRD patterns for chitosan, pure HA, and the prepared composites at different reaction temperatures. Two broad peaks were detected at $2\theta = 11^\circ$ and 20° for pure CS. From the diffraction pattern of HA, the main peaks were observed at $2\theta = 25.7^\circ$, 32.08°, 32.93°, 34.58°, 39.48°, 46.48°, and 49.98°. This was consistent with JCPDS card number 09-0432 and no other calcium phosphate phases were detected indicating that the produced specimens are pure HA. These peaks corresponded to the diffraction plans of (002), (211), (122), (300), (310), (222), and (213), respectively. XRD patterns for chitosan/HA nanocomposite prepared at −10°C, 37°C, and 60°C were represented in traces (c), (d), and (e), respectively (see Figure 1). All characteristic peaks of HA were also detected in the patterns of the composites, whilst CS peaks could not be significantly seen which was suggested to be due to the huge difference in the intensity of the diffraction peaks between HA and CS. This confirms that the in situ prepared calcium phosphates within the composites are exactly HA. Yamaguchi et al. [35] investigated XRD patterns for pure chitosan and CS/HA composites of weight fractions 80/20, 50/50, and 20/80. They assigned the detected peak for CS at 20° to aligned chitosan chains due to intermolecular interactions. They also found that the intensity of this peak decreased for the composites with increasing the amount of HA. This was suggested to be due to the reduction of chemical interaction between chitosan molecules by increasing the HA content. No significant difference was observed in XRD profile between composites prepared at 37°C and 60°C. A considerable change in resolution of the diffraction peaks was observed by changing the reaction temperature from −10 to 60°C (Figure 1). The height of the peaks at $2\theta = 32.9^\circ$ and 34.6° decreased and converted into shoulders in case of the composite prepared at −10°C. This could be ascribed to either a poor crystallinity or a very small crystal size of the produced HA nanoparticles [27, 34]. Similar results were presented by Luo et al. [36] for collagen-chitosan-hydroxyapatite nanocomposites prepared at 4°C. The prepared composites at higher synthesis temperatures (37°C and 60°C) showed similar trends comparing with pure HA. Percentage of crystallinity and crystallite size of

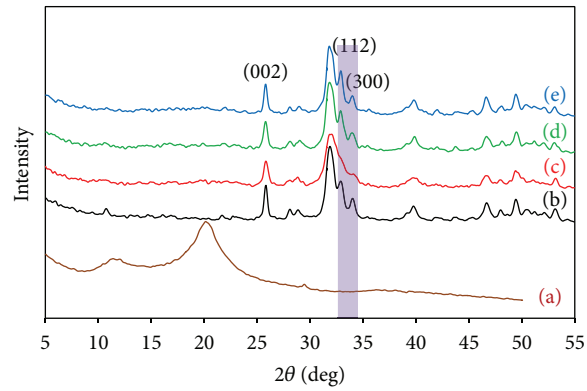

Figure 1: XRD patterns for (a) pure CS, (b) pure HA, (c) CS/HA nanocomposite prepared at −10°C, (d) CS/HA nanocomposite prepared at 37°C, and (e) CS/HA nanocomposite prepared at 60°C.

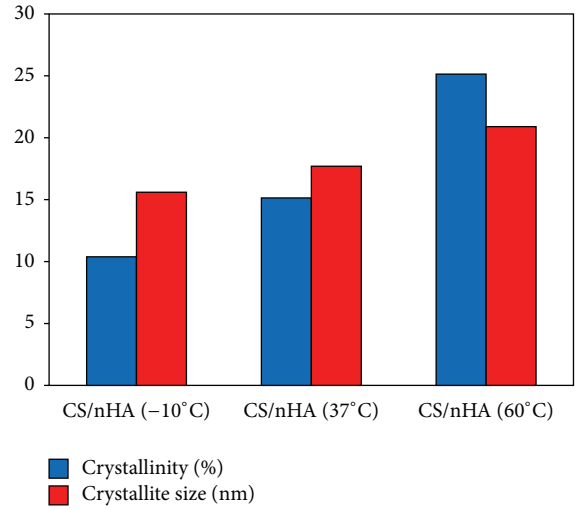

Figure 2: Change in crystallinity and crystallite size for CS/nHA composites prepared at different temperatures (−10, 37, and 60°C).

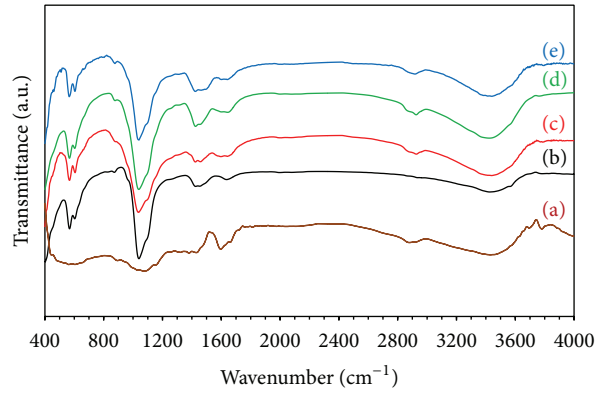

Figure 3: FTIR spectra for (a) pure Cs, (b) pure HA, (c) CS/HA nanocomposite prepared at −10°C, (d) CS/HA nanocomposite prepared at 37°C, and (e) CS/HA nanocomposite prepared at 60°C.

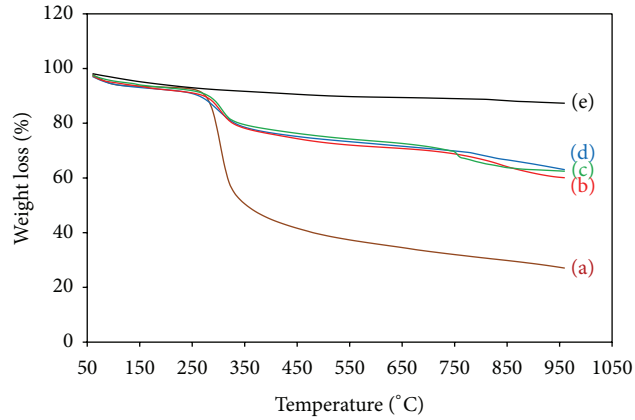

Figure 4: TGA traces for (a) pure Cs, (b) CS/HA nanocomposite prepared at −10°C, (c) CS/HA nanocomposite prepared at 37°C, (d) CS/HA nanocomposite prepared at 60°C, and (e) pure HA.

HA is expected to increase by increasing the processing temperature [21–23, 27].

Figure 2 shows the change in crystallite sizes and percentage of crystallinity for CS/HA nanocomposites produced at different synthesis temperatures. The crystallite size of the HA nanoparticles increased from ~15 nm to ~21 nm with increasing the reaction temperature from −10°C to 60°C. A gradual increase was also seen in crystallinity of the composites from ~10% at −10°C to ~25% at −60°C. Since the average crystallite size and the percentage of crystallinity are inversely proportional to the width at half maximum of (002) reflection of HA, they exhibit a good correlation.

3.2. FTIR Spectroscopy Analysis. The FTIR spectrum of pure chitosan, HA, and CS/HA composites is presented in Figure 3. CS exhibits characteristic bands of peaks that appear around 3360 cm^{-1} corresponding to the stretching vibration of O–H, while 3290 cm^{-1} and 2872 cm^{-1} are due to N–H and C–H asymmetric stretching. The characteristic peaks at 1660 cm^{-1} and 1645 cm^{-1} represent amide I carbonyl stretching (C=O) and amide II (N–H), respectively. The peaks at 1412 cm^{-1} are assigned to the O–H and C–H in the ring. The FTIR spectrum for pure n-HA shows the characteristic bands (see Figure 3) for PO_4^{3-} appeared at 473, 565, 603, 957, 1032, and 1093 cm^{-1}. The broadening of 3000–3500 cm^{-1} bands assigned to (–OH$^-$) stretching of water molecules along with 1647 cm^{-1} assigned to H–O–H bending of molecular water accumulated in the structure was also recorded. The bands at 3570 cm^{-1} and 634 cm^{-1} indicated the hydroxyl stretching (O–H) and librational bending bands. Comparing the FTIR spectrum of pure chitosan and HA with CS-HA composites suggests that characteristic bands of both chitosan and nHA are absolutely present in the composite. The hydroxyl functional group at 3570 cm^{-1} of n-HA disappeared in the spectra of all composites. The disappearance of –OH$^-$ group of n-HA and the movement of polar groups of CS suggest that the hydroxyl group on the surface of n-HA might interact with the plentiful amino and hydroxyl groups of chitosan by the formation of hydrogen bonds.

3.3. Thermal Analysis. The thermal stability of pure Cs, pure n-HA, and Cs/n-HA composites is shown in Figure 4, which plots residual weight versus temperature. The composites were found to be thermally stable in the temperature region between 50 and 250°C. All the traces show a continuous weight loss from 50 to 1000°C. Degradation of chitosan and the composites showed two stages in their TGA curves [37, 38]. The thermal behavior shows a small weight loss in the temperature range from 60 to 100°C and a continuous weight loss from 245 to 450°C. The first degradation stage can be explained by the loss of water and the second stage was ascribed to thermal decomposition of chitosan. When the temperature increased from 250°C to 340°C, the weight decreased sharply with the increasing of temperature because of decomposition of the organic components. The total weight loss for pure chitosan is about 74% due to the polymer degradation. The pure hydroxyapatite is a stable phase up

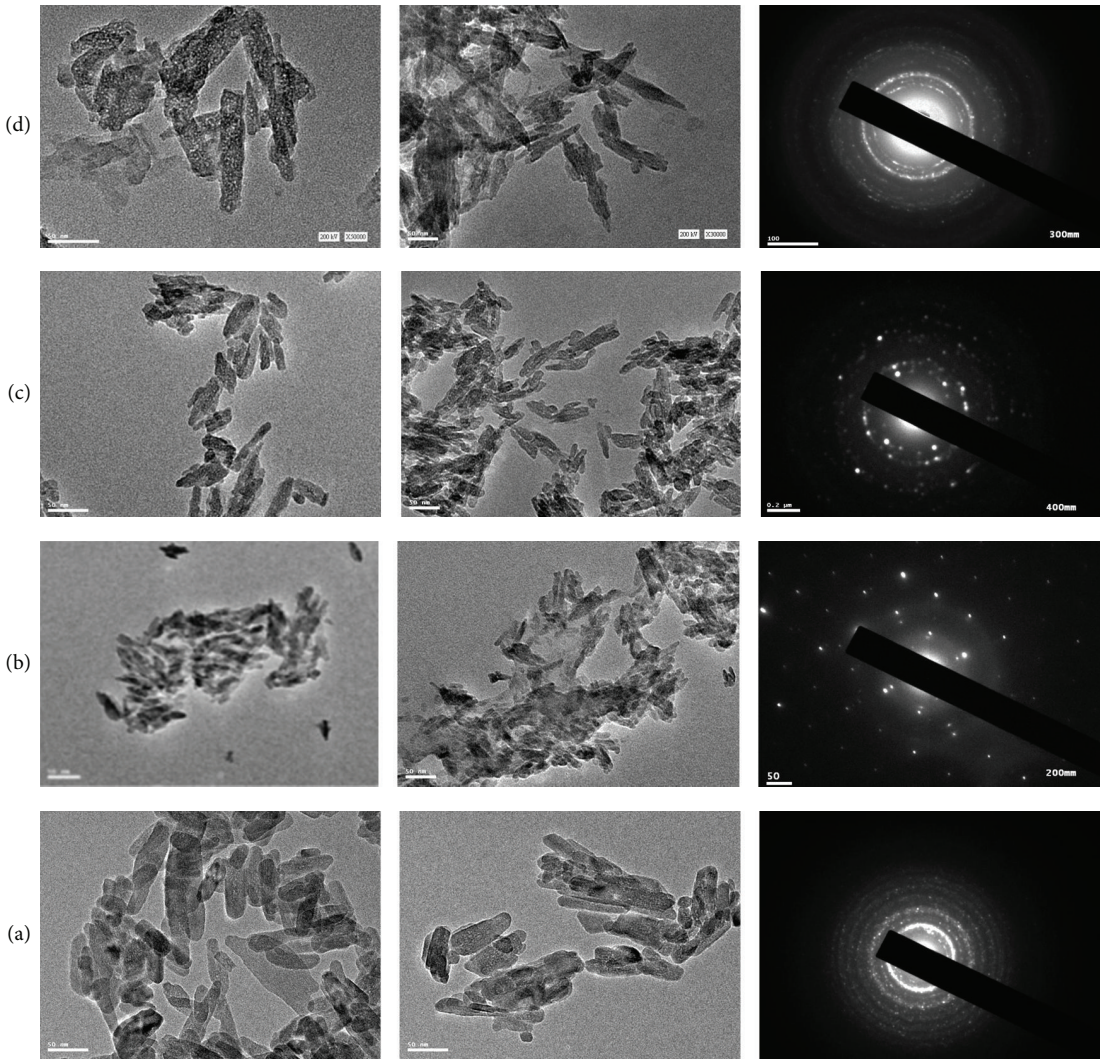

Figure 5: TEM micrographs of (a) pure n-HA, (b) CS/HA nanocomposite prepared at −10°C, (c) CS/HA nanocomposite prepared at 37°C, and (d) CS/HA nanocomposite prepared at 60°C.

to 1200°C [39] and the weight loss that occurred in the composite is due to the chitosan polymer. The incorporation of HA into chitosan improved the thermal stability of the composite because of potential hydrogen bonding between chitosan functional groups and HA crystallites.

3.4. Morphology Observation. The TEM microstructure of nanohydroxyapatite formed within chitosan at different synthesis temperatures is shown in Figure 5. The formation of rod shape of HA in the chitosan polymer matrix can be seen. Some aggregates of needle-shape particles randomly oriented were also observed in the prepared composite at −10°C. Pure n-HA and the prepared composites at 37°C and 60°C are constituted by aggregated rod-like particles. This aggregation was attributed to Van der Waals interaction by Martin et al. [40]. The pure n-HA has hexagonal rod shape with dimensions of ~12–26 nm width and ~32–87 nm length. This size increases as the synthesis temperature increases. The individual particles in the specimen prepared at 60°C showed a rod-like shape with diameter range of 30–50 nm and a length of 80–150 nm. The possible nanoneedle nucleation and growth to the nanorod and consecutive hexagonal transformation could be attributed to the relative specific surface energies, which determine the OH-quantity, associated with the different facets of HA crystal [41]. This was suggested to be due to the fact that the chitosan solution became less viscous at elevated synthesis temperature and can consequently form coordination with metal ions via its amine group. Formation of amine-calcium ions complex is highly suggested for chitosan-hydroxyapatite interaction; however, the interaction of amine groups with calcium is much weaker than transitional metal [35].

From electron diffraction patterns for the CS/HA composites (see Figure 5), sharp rings can be observed corresponding to (002) and (211) lattice planes and indicating assembly of fine nanocrystals appeared at samples (a), (c), and (d) but disappeared at sample b which was confirmed from XRD results. TEM analysis demonstrated that the in

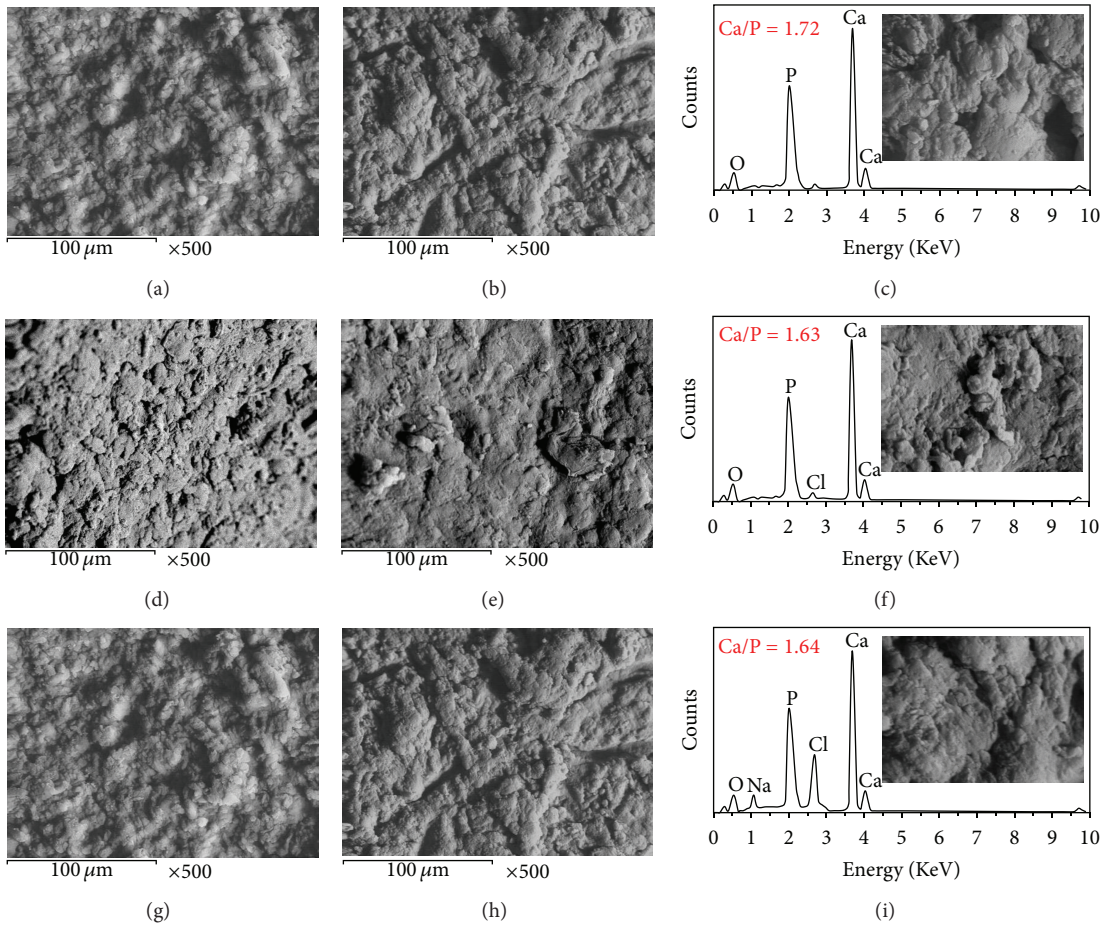

Figure 6: SEM micrographs of the as-prepared composite at (a) 60°C, (d) 37°C, and (g) −10°C. (b), (e), and (h) represent the CS/HA composites prepared at 60°C, 37°C, and −10°C, respectively, after soaking in SBF for 4 weeks at 37°C. EDX patterns can be seen from Figures (c), (f), and (i) for tCS/HA composites prepared at 60°C, 37°C, and −10°C, respectively.

situ prepared apatite particles in the chitosan matrix are in nanosizes.

Examination of apatite formation on a material surface after immersion in SBF is useful for predicting the *in vivo* bone bioactivity of a material. Therefore, the numbers of animals used and the duration of animal experiments can be reduced remarkably [33].

The SEM micrographs of the surface and cross-section of molded composite prepared at different temperatures before and after immersion in SBF for four weeks at 37°C are shown in Figure 6. The surface of composite prepared at −10°C was much rougher than the other composites. SEM of samples surface before immersion in SBF reveal aggregated clusters of hydroxyapatite and chitosan which might refer to the possible conformation change of chitosan chain to random coil at alkaline environment and their ability to envelop HA particle. The hydrogen bond between chitosan chains might cause an approximation between the chains forming the irregular shapes that can be seen in all samples SEM micrographs. It might be possible that the decrease of the temperature during the coprecipitation method might decrease the mobility of the polymer chains forming higher degree of aggregated clusters, as can be monitored by increasing the surface roughness by decreasing the synthesis temperature.

SEM images for the composites after immersion for 4 weeks in a cellular SBF solution-associated EDX area analysis of formed apatite layer revealed that Ca/P molar ratio of the apatite layer was high for the nanocomposite prepared at 60°C in comparison to the other specimens. However, no significant difference in stoichiometry of the apatite layer was detected for the composites prepared at 37 and −10°C. Finally, the formation of a bone-like apatite layer on the surface of the composites after immersion in SBF is indicative of high bioactivity of the produced CS/HA composites.

4. Conclusions

In this work, chitosan/n-HA composites were prepared at different temperatures by a coprecipitation method. The in situ prepared HA particles within the composites were crystalline with nanometer sizes. An excellent miscibility was seen between chitosan and n-HA. Disappearance of other phases of calcium phosphate indicated that the chitosan matrix did not change the crystallographic structure of HA in

the composites but it promoted their crystallization. Decrease in resolution of diffraction peaks at 33° and 34.6° in the XRD pattern for prepared composites at −10°C was attributed to less crystallinity and inhabitation of nHA growth at lower temperatures. This was confirmed from TEM analysis. Increase in the temperature resulted in enhancing the particle size which was ascribed to faster growth rate of HA at higher temperatures in comparison with low temperature (−10°C).

Conflict of Interests

The authors declare that there is no conflict of interests regarding the publication of this paper.

References

[1] K. Y. Lee and S. H. Yuk, "Polymeric protein delivery systems," *Progress in Polymer Science*, vol. 32, no. 7, pp. 669–697, 2007.

[2] K. Rezwan, Q. Z. Chen, J. J. Blaker, and A. R. Boccaccini, "Biodegradable and bioactive porous polymer/inorganic composite scaffolds for bone tissue engineering," *Biomaterials*, vol. 27, no. 18, pp. 3413–3431, 2006.

[3] K. Pielichowska and S. Blazewicz, "Bioactive polymer/hydroxyapatite (nano)composites for bone tissue regeneration," in *Biopolymers*, A. Abe, K. Dusek, and S. Kobayashi, Eds., pp. 97–207, Springer, Berlin, Germany, 2010.

[4] J. E. Block and J. Poser, "Does xenogeneic demineralized bone matrix have clinical utility as a bone graft substitute?" *Medical Hypotheses*, vol. 45, no. 1, pp. 27–32, 1995.

[5] R. C. Sasso, J. I. Williams, N. Dimasi, and P. R. Meyer Jr., "Postoperative drains at the donor sites of iliac-crest bone grafts: a prospective, randomized study of morbidity at the donor site in patients who had a traumatic injury of the spine," *Journal of Bone and Joint Surgery A*, vol. 80, no. 5, pp. 631–635, 1998.

[6] H. K. Uhthoff, P. Poitras, and D. S. Backman, "Internal plate fixation of fractures: short history and recent developments," *Journal of Orthopaedic Science*, vol. 11, no. 2, pp. 118–126, 2006.

[7] R. M. Felfel, I. Ahmed, A. J. Parsons, and C. D. Rudd, "Bioresorbable screws reinforced with phosphate glass fibre: manufacturing and mechanical property characterisation," *Journal of the Mechanical Behavior of Biomedical Materials*, vol. 17, pp. 76–88, 2013.

[8] K. S. Katti, D. R. Katti, and R. Dash, "Synthesis and characterization of a novel chitosan/montmorillonite/hydroxyapatite nanocomposite for bone tissue engineering," *Biomedical Materials*, vol. 3, no. 3, Article ID 034122, 2008.

[9] H. Ehrlich, B. Krajewska, T. Hanke et al., "Chitosan membrane as a template for hydroxyapatite crystal growth in a model dual membrane diffusion system," *Journal of Membrane Science*, vol. 273, no. 1-2, pp. 124–128, 2006.

[10] L. Pighinelli and M. Kucharska, "Properties of microcrystalline chitosan-calcium phosphate complex composite," *Journal of Biomaterials and Nanobiotechnology*, vol. 4, pp. 20–29, 2013.

[11] A. Sabokbar, R. Pandey, J. Díaz, J. M. W. Quinn, D. W. Murray, and N. A. Athanasou, "Hydroxyapatite particles are capable of inducing osteoclast formation," *Journal of Materials Science*, vol. 12, no. 8, pp. 659–664, 2001.

[12] A. E. Elçin, Y. M. Elçin, and G. D. Pappas, "Neural tissue engineering: adrenal chromaffin cell attachment and viability on chitosan scaffolds," *Neurological Research*, vol. 20, no. 7, pp. 648–654, 1998.

[13] M. Peter, N. Ganesh, N. Selvamurugan et al., "Preparation and characterization of chitosan-gelatin/nanohydroxyapatite composite scaffolds for tissue engineering applications," *Carbohydrate Polymers*, vol. 80, no. 3, pp. 687–694, 2010.

[14] K. Sahithi, M. Swetha, M. Prabaharan et al., "Synthesis and characterization of nanoscale-hydroxyapatite-copper for antimicrobial activity towards bone tissue engineering applications," *Journal of Biomedical Nanotechnology*, vol. 6, no. 4, pp. 333–339, 2010.

[15] S. K. Misra, D. Mohn, T. J. Brunner et al., "Comparison of nanoscale and microscale bioactive glass on the properties of P(3HB)/Bioglass composites," *Biomaterials*, vol. 29, no. 12, pp. 1750–1761, 2008.

[16] M. Wang, R. Joseph, and W. Bonfield, "Hydroxyapatite-polyethylene composites for bone substitution: effects of ceramic particle size and morphology," *Biomaterials*, vol. 19, no. 24, pp. 2357–2366, 1998.

[17] J. Li, X. L. L. X.L.Lu, and Y. F. Zheng, "Effect of surface modified hydroxyapatite on the tensile property improvement of HA/PLA composite," *Applied Surface Science*, vol. 255, no. 2, pp. 494–497, 2008.

[18] Z. Hong, X. Qiu, J. Sun, M. Deng, X. Chen, and X. Jing, "Grafting polymerization of L-lactide on the surface of hydroxyapatite nano-crystals," *Polymer*, vol. 45, no. 19, pp. 6699–6706, 2004.

[19] E. T. Thostenson, Z. Ren, and T.-W. Chou, "Advances in the science and technology of carbon nanotubes and their composites: a review," *Composites Science and Technology*, vol. 61, no. 13, pp. 1899–1912, 2001.

[20] I. M. Pelin, I. Popescu, D. M. Suflet, M. Aflori, and V. Bulacovschi, "Influence of maleic acid copolymers on calcium orthophosphates crystallization at low temperature," *Journal of Crystal Growth*, vol. 377, pp. 127–135, 2013.

[21] Y. X. Pang and X. Bao, "Influence of temperature, ripening time and calcination on the morphology and crystallinity of hydroxyapatite nanoparticles," *Journal of the European Ceramic Society*, vol. 23, no. 10, pp. 1697–1704, 2003.

[22] T. Furuzono, D. Walsh, K. Sato, K. Sonoda, and J. Tanaka, "Effect of reaction temperature on the morphology and size of hydroxyapatite nanoparticles in an emulsion system," *Journal of Materials Science Letters*, vol. 20, no. 2, pp. 111–114, 2001.

[23] R. Kumar, K. H. Prakash, P. Cheang, and K. A. Khor, "Temperature driven morphological changes of chemically precipitated hydroxyapatite nanoparticles," *Langmuir*, vol. 20, no. 13, pp. 5196–5200, 2004.

[24] C. Kothapalli, M. Wei, A. Vasiliev, and M. T. Shaw, "Influence of temperature and concentration on the sintering behavior and mechanical properties of hydroxyapatite," *Acta Materialia*, vol. 52, no. 19, pp. 5655–5663, 2004.

[25] A. S. Milev, G. S. K. Kannangara, B. Ben-Nissan, and M. A. Wilson, "Temperature effects on a hydroxyapatite precursor solution," *Journal of Physical Chemistry B*, vol. 108, no. 18, pp. 5516–5521, 2004.

[26] A. Zanotto, M. Saladino, D. Martino, and E. Caponetti, "Influence of temperature on calcium hydroxyapatite nanopowders," *Advances in Nanoparticles*, vol. 1, pp. 21–28, 2012.

[27] G. A. Martínez-Castañón, J. P. Loyola-Rodríguez, and N. V. Zavala-Alonso, "Preparation and characterization of nanostructured powders of hydroxyapatite," *Superficies y Vacío*, vol. 25, pp. 101–105, 2012.

[28] M. N. Salimi, R. H. Bridson, L. M. Grover, and G. A. Leeke, "Effect of processing conditions on the formation of hydroxyapatite nanoparticles," *Powder Technology*, vol. 218, pp. 109–118, 2012.

[29] W. Feng, L. Mu-Sen, L. Yu-Peng, and Q. Yong-Xin, "A simple sol-gel technique for preparing hydroxyapatite nanopowders," *Materials Letters*, vol. 59, no. 8-9, pp. 916–919, 2005.

[30] M. H. Fathi and A. Hanifi, "Evaluation and characterization of nanostructure hydroxyapatite powder prepared by simple sol-gel method," *Materials Letters*, vol. 61, no. 18, pp. 3978–3983, 2007.

[31] M. H. Fathi, A. Hanifi, and V. Mortazavi, "Preparation and bioactivity evaluation of bone-like hydroxyapatite nanopowder," *Journal of Materials Processing Technology*, vol. 202, no. 1–3, pp. 536–542, 2008.

[32] V. M. Rusu, C.-H. Ng, M. Wilke, B. Tiersch, P. Fratzl, and M. G. Peter, "Size-controlled hydroxyapatite nanoparticles as self-organized organic-inorganic composite materials," *Biomaterials*, vol. 26, no. 26, pp. 5414–5426, 2005.

[33] T. Kokubo and H. Takadama, "How useful is SBF in predicting in vivo bone bioactivity?" *Biomaterials*, vol. 27, no. 15, pp. 2907–2915, 2006.

[34] Z. Li, L. Yubao, Y. Aiping, P. Xuelin, W. Xuejiang, and Z. Xiang, "Preparation and in vitro investigation of chitosan/nano-hydroxyapatite composite used as bone substitute materials," *Journal of Materials Science: Materials in Medicine*, vol. 16, no. 3, pp. 213–219, 2005.

[35] I. Yamaguchi, K. Tokuchi, H. Fukuzaki et al., "Preparation and microstructure analysis of chitosan/hydroxyapatite nanocomposites," *Journal of Biomedical Materials Research*, vol. 55, pp. 20–27, 2001.

[36] D. Luo, L. Sang, X. Wang, S. Xu, and X. Li, "Low temperature, pH-triggered synthesis of collagen-chitosan-hydroxyapatite nanocomposites as potential bone grafting substitutes," *Materials Letters*, vol. 65, no. 15-16, pp. 2395–2397, 2011.

[37] F. A. A. Tirkistani, "Thermal analysis of some chitosan Schiff bases," *Polymer Degradation and Stability*, vol. 60, no. 1, pp. 67–70, 1998.

[38] C. Qin, B. Zhou, L. Zeng et al., "The physicochemical properties and antitumor activity of cellulase-treated chitosan," *Food Chemistry*, vol. 84, no. 1, pp. 107–115, 2004.

[39] I. Manjubala, S. Scheler, J. Bössert, and K. D. Jandt, "Mineralisation of chitosan scaffolds with nano-apatite formation by double diffusion technique," *Acta Biomaterialia*, vol. 2, no. 1, pp. 75–84, 2006.

[40] C. L. Martin, D. Bouvard, and G. Delette, "Discrete element simulations of the compaction of aggregated ceramic powders," *Journal of the American Ceramic Society*, vol. 89, no. 11, pp. 3379–3387, 2006.

[41] K. P. Sanosh, M.-C. Chu, A. Balakrishnan, Y.-J. Lee, T. N. Kim, and S.-J. Cho, "Synthesis of nano hydroxyapatite powder that simulate teeth particle morphology and composition," *Current Applied Physics*, vol. 9, no. 6, pp. 1459–1462, 2009.